# Diurnal Characteristics of Precipitation Features over the Tropical East Pacific: A Comparison of the EPIC and TEPPS Regions

R. CIFELLI

*Colorado State University, Fort Collins, Colorado*

S. W. NESBITT

*University of Illinois at Urbana–Champaign, Urbana, Illinois*

S. A. RUTLEDGE

*Colorado State University, Fort Collins, Colorado*

W. A. PETERSEN

*University of Alabama in Huntsville, Huntsville, Alabama*

S. YUTER

*North Carolina State University at Raleigh, Raleigh, North Carolina*

(Manuscript received 1 May 2007, in final form 1 November 2007)

ABSTRACT

This study examines the diurnal cycle of precipitation features in two regions of the tropical east Pacific where field campaigns [the East Pacific Investigation of Climate Processes in the Coupled Ocean–Atmosphere System (EPIC) and the Tropical Eastern Pacific Process Study (TEPPS)] were recently conducted. EPIC (10°N, 95°W) was undertaken in September 2001 and TEPPS (8°N, 125°W) was carried out in August 1997. Both studies employed C-band radar observations on board the NOAA ship *Ronald H. Brown* (*RHB*) and periodic upper-air sounding launches to observe conditions in the surrounding environment. Tropical Rainfall Measuring Mission (TRMM) Precipitation Radar (PR) and Geostationary Operational Environmental Satellite (GOES) IR data are used to place the *RHB* data in a climatological context and Tropical Atmosphere Ocean (TAO) buoy data are used to evaluate changes in boundary layer fluxes in context with the observed diurnal cycle of radar observations of precipitation features.

Precipitation features are defined as contiguous regions of radar echo and are subdivided into mesoscale convective system (MCS) and sub-MCS categories. Results show that MCSs observed in EPIC and TEPPS have distinct diurnal signatures. Both regions show an increase in intensity starting in the afternoon hours, with the timing of maximum rain intensity preceding maxima in rain area and accumulation. In the TEPPS region, MCS rain rates peak in the evening and rain area and accumulation in the late night–early morning hours. In contrast, EPIC MCS rain rates peak in the late night–early morning, and rain area and accumulation are at a maximum near local sunrise. The EPIC observations are in agreement with previous satellite studies over the Americas, which show a phase lag response in the adjacent oceanic regions to afternoon–evening convection over the Central American landmass. Sub-MCS features in both regions have a broad peak extending through the evening to late night–early morning hours, similar to that for MCSs. During sub-MCS-only periods, the rainfall patterns of these features are closely linked to diurnal changes in SST and the resulting boundary layer flux variability.

*Corresponding author address:* Robert Cifelli, Department of Atmospheric Science, Colorado State University, Fort Collins, CO 80523-1371.
E-mail: rob@atmos.colostate.edu

DOI: 10.1175/2007JCLI2020.1

## 1. Introduction

It is well known that tropical convection has a significant impact on global climate. In particular, studies have shown that precipitation and latent heating in tropical convection affect the large-scale circulation through heat and moisture transports (Riehl and Malkus 1958; Hartmann et al. 1984; DeMaria 1985). Although tropical convection and precipitation processes vary over a broad range of time scales, the fundamental mode of variability is driven by the daily change in solar insolation (Hendon and Woodberry 1993). Indeed, it has been argued that the ability to accurately simulate the diurnal cycle of precipitation is a fundamental test of a numerical climate model (Lin et al. 2000; Yang and Slingo 2001; Dai and Trenberth 2004). One region of intense interest in this vein is the tropical east Pacific ITCZ, which exhibits strong zonal variations in precipitation and atmospheric circulation (Janowiak et al. 1995) and is an area over which two recent field campaigns were conducted: the East Pacific Investigation of Climate Processes in the Coupled Ocean–Atmosphere System (EPIC-2001; Raymond et al. 2004) and the Tropical Eastern Pacific Process Study (TEPPS; Yuter and Houze 2000).

Precipitation diurnal variations in the tropics have been studied extensively (e.g., Gray and Jacobson 1977; Hendon and Woodberry 1993; Garreaud and Wallace 1997; Chen et al. 1996; Sui et al. 1997; Dai 2001; Yang and Slingo 2001; Bowman et al. 2005; and many others). A number of forcing mechanisms have been proposed to account for the diurnal cycle (see Yang and Smith 2006 for a recent literature review). The majority of observational studies, using data ranging from rain gauge and ship reports to radar and satellite data, have shown that precipitation diurnal variations are pronounced over land during the warm season, with a maximum in precipitation occurring in the late afternoon–early evening occurring in most (but not all) areas associated with changes in solar insolation (e.g., see Dai 2001). Over the oceans, however, the signal is weaker than over the continents and the phase is more variable, although an early morning maximum is seen over most open-ocean regions (Houze et al. 1981; Janowiak et al. 1994; Dai 2001; Yang and Slingo 2001; Nesbitt and Zipser 2003; Johnson et al. 2004; also see Fig. 1). As pointed out by Yang and Slingo (2001) and exemplified in Fig. 1, many oceanic regions near coastlines appear to have diurnal signals correlated with land-based convection, coupled through gravity wave currents and/or land–sea breeze interactions. Mapes et al. (2003) used a simple numerical model to show how diurnal heating over elevated terrain in the Panama Bight region could excite gravity waves and lead to the subsequent onset of precipitation over the adjacent ocean region. These previous works lead us to the hypothesis that the proximity to land of an ocean location is an important driver in determining the local phase of the diurnal cycle resulting from either the propagation of convective systems or external nonconvective forcing such as gravity waves.

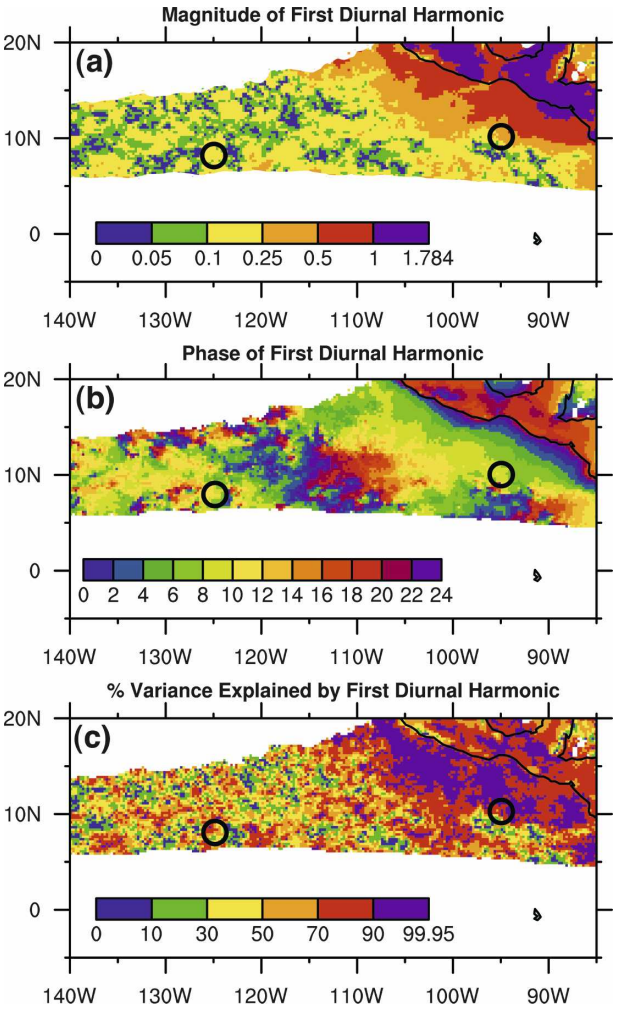


FIG. 1. Harmonic analysis of the TRMM combined 3B42 rain-rate product for June–August 1998–2005. The rain-rate time series was analyzed at each grid point (0.5° × 0.5° resolution where the rain rate ≥ 3 mm day$^{-1}$) for its amplitude, phase of maximum, and percent variance explained by the Fourier analysis in the raw time series: (a) magnitude of the diurnal cycle, (b) phase (LT), and (c) percent variance of the mean diurnal cycle explained by the first diurnal harmonic. The amplitude is expressed as a fractional variance of the maximum divided by the mean. The black circles indicate the EPIC (10°N, 95°W) and TEPPS (8°N, 125°W) regions.

Over the open ocean, studies regarding the diurnal

cycle of precipitation are often hampered by the paucity of observations (Dai 2001). This is particularly true in the east Pacific ITCZ region, where atmospheric–oceanic processes are poorly represented in numerical models (Mechoso et al. 1995; Raymond et al. 2003) and large discrepancies between the simulated and observed diurnal cycle of precipitation exist (Yang and Slingo 2001, their Figs. 3 and 8; Dai and Trenberth 2004, their Fig. 12). The Yang and Slingo study used infrared (IR) brightness temperature data to infer precipitation, and the Dai and Trenberth study used Comprehensive Ocean–Atmosphere Data Set (COADS) surface reports to estimate precipitation. Given the crude relationship between IR brightness temperature and rainfall at the surface (e.g., Arkin and Meisner 1987; Yuter and Houze 1998), the paucity of surface reports in remote ocean regions of the east-central Pacific (Dai 2001), and limitations of GCMs in producing important convective feedback in the ocean–atmosphere system (Arakawa 2004), it is not surprising that discrepancies between the models and observations exist. Moreover, as discussed below, the relative weakness of the observed diurnal signal over open-ocean regions as compared to land and coastal areas has important practical implications for model validation studies of the diurnal cycle (Fig. 1).

Serra and McPhaden (2004) examined buoy data from the tropical Pacific and Atlantic Oceans between 1997 and 2001 to explore the diurnal cycle of precipitation as a function of season (June–December versus January–May) and region. They found that buoys in the northeast Pacific indicate both late morning–early afternoon and early morning peaks in rainfall accumulation and intensity during the June–December period. The early morning peak was attributed to rainfall from deep, organized systems; the noon peak was assumed to be caused by small, unorganized systems. However, the late morning–early afternoon peak was not present at all buoy locations (most notably at the EPIC ITCZ location at 10°N, 95°W), and the study did not attempt to discriminate rainfall characteristics within the broad east Pacific region (90°–140°W). Bowman et al. (2005) also used multiyear buoy data in the tropical Pacific as well as corresponding Tropical Rainfall Measuring Mission (TRMM) Microwave Imager (TMI) and Precipitation Radar (PR) data to examine the diurnal cycle of rainfall. They found a consistent early morning rainfall peak in both the satellite and buoy datasets. The satellite estimates generally showed less geographic variability in the diurnal signal compared to the buoy gauges, which the authors attributed to better spatial sampling by TRMM.

As noted above, the EPIC and TEPPS campaigns were conducted to improve the understanding of ocean–atmosphere processes in the east-central Pacific. Both regions have been shown to be impacted by a variety of tropical wave disturbances, including easterly waves (Kiladis and Wheeler 1995; Straub and Kiladis 2002; Serra and Houze 2002; Petersen et al. 2003). Pereira and Rutledge (2006) examined the diurnal cycle of convection during northerly (ahead of easterly wave troughs) and southerly (behind easterly wave troughs) regimes in the EPIC region. They found that convection in the northerly regime was more intense than in the southerly regime (as revealed by vertical radar reflectivity structure; consistent with Petersen et al. 2003) and that convection in the northerly phase peaked around midnight compared to near dawn in the southerly phase.

In this study, we utilize the EPIC and TEPPS observations to explore the diurnal cycle of precipitation in these regions within the tropical east Pacific. We draw data from a variety of platforms, including ship-based radar, upper-air soundings, and buoy and satellite observations. Our goal is to quantify the precipitation diurnal cycle characteristics in this poorly sampled region of the tropics and to determine how well the field program data collected in these two locations represent longer-term climatologies from satellite data. This study complements the previous work of Cifelli et al. (2007, hereafter CNR07), which examined the overall characteristics of precipitation in the EPIC and TEPPS regions from a ship and satellite perspective; however, Cifelli et al. did not analyze the diurnal cycle.

The paper is organized as follows: Section 2 outlines the methodology used to compare the various datasets as well as how the field program data are further subdivided into sub-mesoscale convective system (sub-MCS) only time periods. Section 3 describes the diurnal cycle observed during the field campaign from an environmental perspective (buoys and soundings), provides radar statistics of precipitation, and uses satellite data to place the field campaign data within a climatological context. Section 4 presents some concluding remarks and suggestions for future study.

## 2. Methodology

Ship radar data and upper-air sounding data were collected aboard the NOAA research vessel *Ronald H. Brown* (*RHB*) during both the TEPPS and EPIC-2001 campaigns. TEPPS was conducted during 8–23 August 1997 and EPIC-2001 during 11 September–1 October 2001. The radar and upper-air sounding data were

processed in a similar fashion to that described in CNR07 (only a brief description will be provided here). The ship radar data were interpolated to a 3-km horizontal and vertical resolution out to 110 km from the location of the nominal ship position in the EPIC and TEPPS campaigns (10°N, 95°W and 7.8°N, 125°W, respectively). Because of the relatively wide antenna beamwidth of the *RHB* radar during TEPPS, 3 km was chosen as the minimum spacing to preserve the native radar data resolution at maximum range (CNR07). An objective algorithm was used to identify contiguous echo regions at reflectivity thresholds $\geq$10 dB$Z$. The features were subdivided into MCSs [areas equal or exceeding 1000 km$^2$ with at least 1 pixel (9 km$^2$) identified as convective], sub-MCSs (areas less than 1000 km$^2$ with at least one convective pixel), and nonconvective systems (NCs) (NC – features of any size with no convective pixels). In this study, we focus on sub-MCS and MCS because NCs do not contribute significantly to rainfall accumulations (CNR07). Vertical and horizontal feature properties (e.g., area, rain rate, and mean maximum echo top height) were determined for each volume of radar data collected and then composited within 6-h time bins to examine diurnal cycle characteristics. Although there was sufficient sampling to composite the radar data at smaller temporal resolution, the 6-h time bins were established as a compromise to preserve sufficient samples in each time block while exposing variability in the diurnal parameters at equal temporal resolution among all datasets.

Upper-air soundings were acquired 6 times day$^{-1}$ during both experiments; these data were used to characterize the thermodynamic characteristics of the environment. A total of 113 and 91 soundings were available for the EPIC and TEPPS campaigns, respectively. The sonde data went through quality control at the Joint Office for Science Support (JOSS) at the National Center for Atmospheric Research (NCAR), using methods similar to those used to quality control the Tropical Ocean and Global Atmosphere Coupled Ocean–Atmosphere Response Experiment (TOGA COARE) sounding data (Loehrer et al. 1996). The convective available potential energy (CAPE) and convective inhibition (CIN) were calculated (in J kg$^{-1}$), assuming a 50-mb mixed layer and pseudoadiabatic ascent with no contribution from ice processes.

Data from the Tropical Atmosphere Ocean/Triangle Trans-Ocean Buoy Network (TAO/TRITON; McPhaden et al. 1998) were used to establish background properties [e.g., sea surface temperature (SST), air temperature, mixing ratio, and wind speed] as well as sensible and latent heat fluxes at the TEPPS and EPIC locations. For the EPIC and TEPPS buoys, SST was measured at a depth of 1 m, and air temperature, wind, and relative humidity were measured at 3–4 m (see http://www.pmel.noaa.gov/tao/proj_over/mooring.shtml). The calculation of surface fluxes from the TAO buoy data is described in Cronin et al. (2006).

TRMM satellite data were also used to help place the ship-based observations within the context of a multiyear time series. TRMM 3B42 combined data for July, August, and September 1998–2005 were utilized to construct a harmonic analysis of diurnal rainfall over the east-central Pacific region and examine the influence of land-based convection on the region.[1] The TRMM PR version 6 product was analyzed to develop diurnal statistics of rainfall properties over the EPIC and TEPPS regions as described in CNR07. The version 6 product has a gridded resolution of 4.2 km before August 2001 and 4.5 km afterward. All data acquired 1998–2004 (July–September) within 5° $\times$ 5° boxes centered on the nominal location of the field programs were used to determine the same precipitation characteristics as the *RHB* over the EPIC and TEPPS domains. The TRMM PR data were composited into 6-h time bins to reduce noise in the resulting parameter statistics. Effects of area averaging of TRMM data are discussed in Bowman et al. (2005). In general, the magnitude of the diurnal signal is reduced as the size of the TRMM sampling region is increased. Sensitivity studies showed that there was little difference in the resulting characteristics at either 10° $\times$ 10° or 5° $\times$ 5° boxes when using 6-h time bins.

Merged IR satellite data, available from the National Aeronautics and Space Administration (NASA) Goddard Distributed Active Archive Center (DAAC), were also used for this study. This dataset was developed by the National Atmospheric and Oceanic Administration (NOAA) Climate Prediction Center and consists of IR brightness temperature data at 4-km horizontal resolution from 60°N–60°S, analyzed at half-hourly resolution (Janowiak et al. 2001). For this study, data from July–September for 2000–05 (all years available) were extracted for the same 5° $\times$ 5° boxes surrounding the nominal locations of the EPIC and TEPPS field programs that were used for the TRMM PR data. Brightness temperature distributions at 6-h

[1] The TRMM 3B42 is a 3-hourly product produced through an optimal combination of SSMI, TRMM TMI, AMSU, and AMSR precipitation estimates. (See http://daac.gsfc.nasa.gov/precipitation/TRMM_README/TRMM_3B42_readme.shtml for more information).

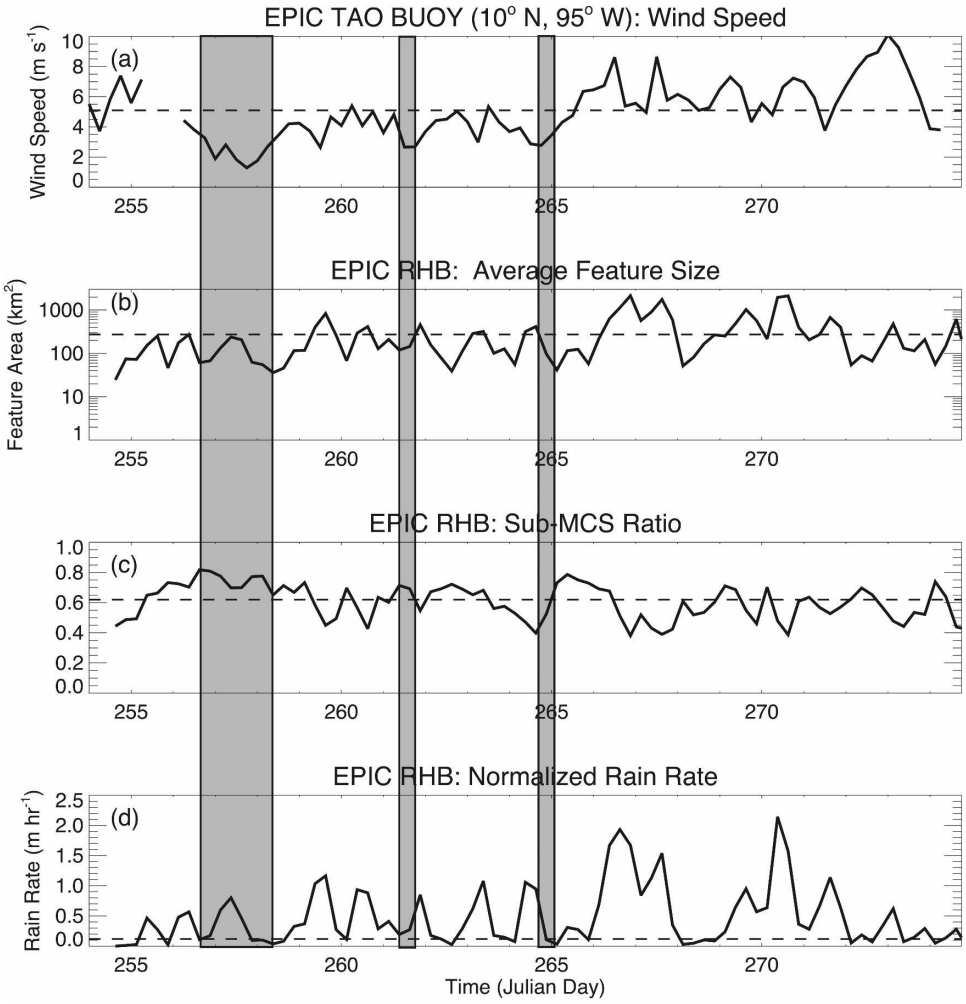


FIG. 2. Time series of selected TAO buoy and radar statistics for the EPIC campaign at 6-h time resolution: (a) buoy wind speed ($m\,s^{-1}$), (b) average precipitation feature size ($km^2$), (c) ratio of sub-MCS to total feature occurrence, and (d) conditional rain rate normalized to the entire radar domain ($mm\ h^{-1}$); (b)–(d) are based on *RHB* radar data. Shaded regions denote approximate SMO time periods; horizontal lines show average quantities during the field campaign.

intervals were calculated to compare the distribution of cloud top temperatures to the *RHB* radar statistics.

### *Sub-MCS-only regime classification*

It was of interest to examine the diurnal cycle of both thermodynamic and radar characteristics during the entire course of the field experiments as well as within time periods of relatively unorganized activity. In this study, time intervals in which the TAO buoy data indicated relatively light winds ($\leq 3.5\ m\,s^{-1}$) and the radar data indicated a lack of large-scale organization of precipitation across the domain (i.e., MCSs did not occur) were defined as sub-MCS-only (SMO) conditions. These periods were identified using time series of 6-h averaged wind speed and feature size (see Figs. 2 and 3). As expected, these time intervals generally contained a relatively high fraction of sub-MCS features and low rain rates. SMO conditions were rare during EPIC compared to TEPPS (see Table 1). Moreover, two of the EPIC SMO periods (Julian dates 256–258 and 264–265) corresponded to dry layer intrusion episodes over the east tropical Pacific (Zuidema et al. 2006). These episodes were marked by reduced relative humidity in the middle troposphere and a reduction in cloud vertical structure (Zuidema et al. 2006; CNR07). Because of the smaller number of samples, the results for the SMO periods are noisier compared to the total, and caution must be applied when interpreting these category results. Nevertheless, the results are shown to

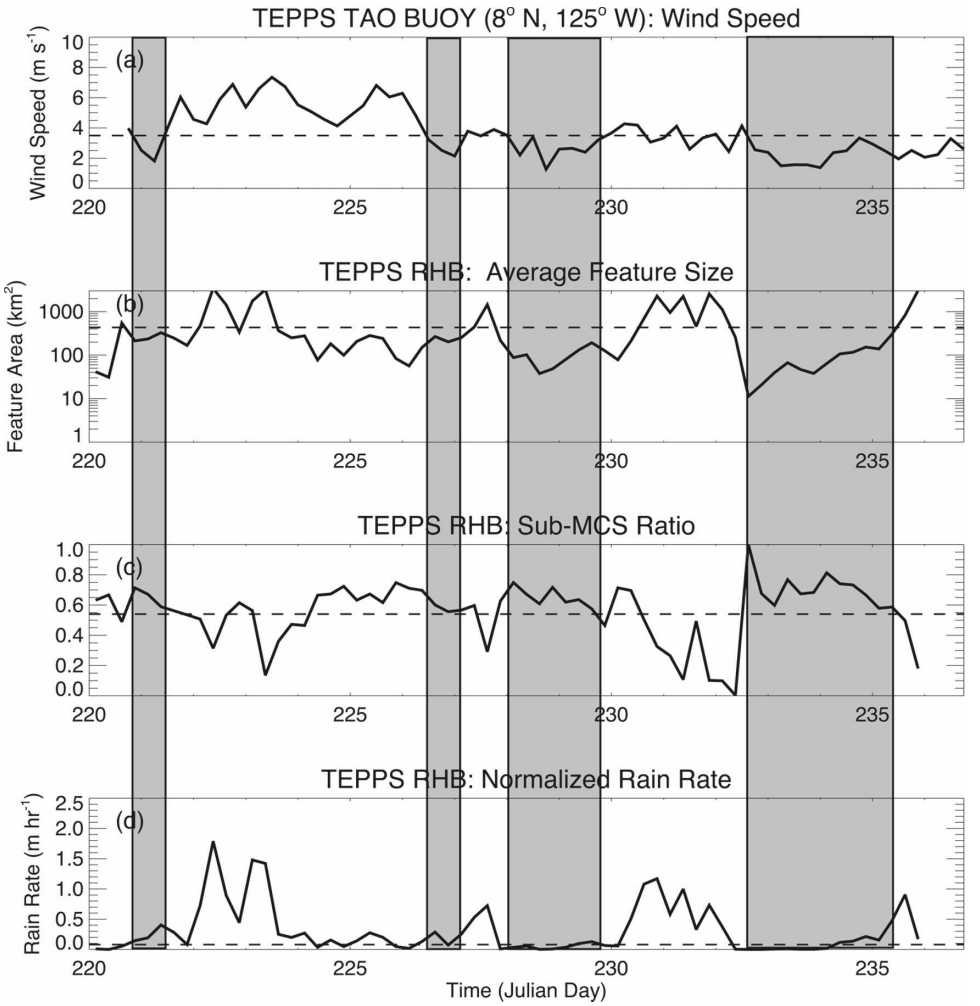


FIG. 3. Same as Fig. 2, but for the TEPPS field campaign.

illustrate diurnal cycle variability with changes in large-scale forcing and to allow comparison with previous works from other geographic locations. (We will hereafter refer to analyses from the entire field campaigns as "all-data" and analyses from SMO periods as "SMO data".)

## 3. Results

The large-scale environmental characteristics of the EPIC and TEPPS regions are discussed in CNR07, and only a brief review will be presented here. Both the EPIC and TEPPS regions are located in the east Pacific warm pool with boreal summer mean SSTs generally above 27°C (see Fig. 1 of CNR07). However, the EPIC region is located more centrally to the warm pool; TEPPS is situated along the fringe at the western end, in closer proximity to the equatorial cold tongue. Satellite-observed outgoing longwave radiation (OLR) brightness temperatures are generally lower at the eastern end of the warm pool, closer to the Central America landmass where the EPIC campaign was conducted. These results are consistent with field campaign data, indicating a pattern of deeper, more electrified convection and heavier precipitation in the EPIC region than in TEPPS. Because TEPPS was conducted during an El Niño year, SSTs and resulting precipitation activity [as shown in the OLR climatology of CNR07, Su et al. (2001), and Su and Neelin (2003)] were more intense across the TEPPS region compared

TABLE 1. Hours of observations in each field program. Numbers in parentheses refer to the percentage of total.

| Field program | Total hours of observations | Total hours of observations: SMO periods |
|---|---|---|
| EPIC | 491 | 60 (12%) |
| TEPPS | 383 | 132 (34%) |

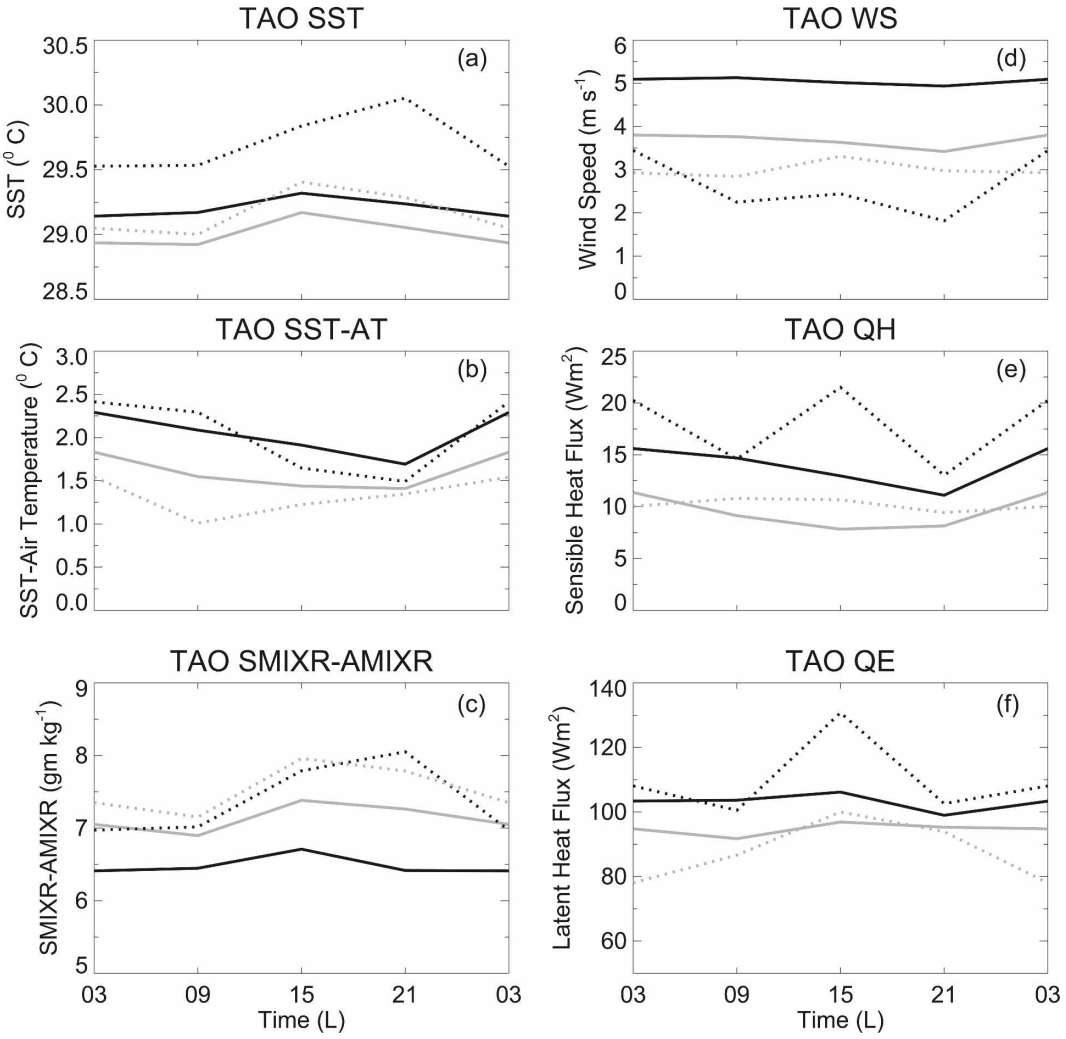


FIG. 4. TAO buoy parameters for EPIC (black) and TEPPS (gray). Solid lines indicate all data collected during the field programs; short dashed lines indicate SMO conditions (i.e., wind speeds $<3.5$ m s$^{-1}$ at the buoy and no large-scale organization of radar echoes). (a) Sea surface temperature (°C), (b) sea–air temperature difference (°C), (c) sea–air mixing ratio difference (g kg$^{-1}$), (d) wind speed (m s$^{-1}$), (e) sensible heat flux (W m$^{-2}$), and (f) latent heat flux (W m$^{-2}$).

to climatology. However, despite the El Niño conditions, CNR07 showed that the EPIC precipitation during the field program was more intense in terms of vertical structure, with larger MCSs and a greater contribution of precipitation coming from ice processes compared to TEPPS.

### *a. Diurnal cycle characteristics of the environment*

We begin by examining the diurnal cycle of select environmental parameters during each of the field programs. Figure 4 shows the diurnal pattern for selected parameters and derived fluxes from the TAO/TRITON buoys at 10°N, 95°W (EPIC) and 8°N, 125°W (TEPPS). The sampling points shown in Fig. 4 and subsequent diurnal cycle plots are located at the center of the 6-h time bin and will be referred to throughout the paper as follows: late night–early morning (0300 LT), midmorning (0900 LT), midafternoon (1500 LT), and evening (2100 LT).

When the all-data case is considered, the diurnal variability of buoy parameters is small in both regions (Fig. 4). On average, the measured parameters and derived fluxes are higher in EPIC compared to TEPPS. SST exhibits a small afternoon increase, in phase with changes in solar insolation (Fig. 4a). A similar trend occurs in air temperature (not shown). Differences between SST and air temperature are highest in the late night–early morning (Fig. 4b), which contributes to the

corresponding maximum in bulk sensible heat flux (Fig. 4e). There is little diurnal variability in the air–sea mixing ratio (Fig. 4c) or wind speed (Fig. 4d); therefore, the resulting latent heat flux variability in both regions is also small (Fig. 4f).

When the buoy fluxes are examined in SMO periods, the diurnal amplitudes are greater and differences between the EPIC and TEPPS regions become more apparent. In EPIC, SST increases about 0.5°C throughout the daylight hours, with maximum amplitude occurring in the evening (Fig. 4a).[2] The corresponding TEPPS SST response is damped with respect to EPIC, with a maximum occurring in midafternoon. The smaller diurnal amplitude of SST in the SMO TEPPS buoy data may be attributable to the El Niño conditions that occurred during the TEPPS experiment. Previous work by Cronin and Kessler (2002) examined mixed layer variability at a different TAO buoy (0°, 110°W) for a time period that included the 1997/98 El Niño. The authors found that the diurnal cycle of SST was reduced during the warm phase El Niño as a consequence of changes in the mixed layer depth.[3]

Compared to the all-data results, the increased SST response in both regions during SMO periods is similar to observations in the west Pacific warm pool (Sui et al. 1997; Johnson et al. 2001). The larger SSTs contribute to enhanced sensible and latent heat fluxes during SMO periods compared to the all-data plots (Figs. 4e,f), especially in the EPIC region. As described below in section 3b, the diurnal patterns in SST during SMO periods were mirrored by changes in sub-MCS precipitation characteristics.

The daily variability of selected upper-air sounding parameters is shown in Fig. 5. Because of the relatively small number of soundings, only all-data plots are shown. We emphasize that the thermodynamic parameters are statistical composites and are not necessarily representative of the inflow air for a particular feature. Rather, the composites shown in Fig. 5 reflect trends in the environment that may be affected by downdrafts and/or evaporation from precipitation features near the sensor and that therefore may have some relationship with the types of precipitation features observed during those time periods. CAPE is larger in EPIC across the diurnal cycle (Fig. 5a), which is consistent with the echo top height statistics presented below in section 3b. In both regions, CAPE decreases through the morning, achieving a minimum in the midafternoon hours. In EPIC, CAPE is maximized in the late night–early morning. A similar pattern is observed in the TEPPS region, although with smaller amplitude variability and a slight preference for an evening maximum. As discussed below, the CAPE peak in both regions is essentially coincident with the peak in rain rate from MCS-scale systems. Because MCSs supply the bulk of the rainfall in EPIC and TEPPS (CNR07), this suggests a strong correlation between the diurnal cycle of CAPE and rainfall, similar to observations from the west Pacific warm pool region (Petersen et al. 1996). During easterly wave passages observed in the EPIC campaign, Petersen et al. (2003) showed that enhancements in surface sensible and latent heat fluxes preceded corresponding increases in CAPE. Based on comparisons of Figs. 4 and 5, there may be some correlation between sensible heat fluxes and CAPE on diurnal time scales, but it is not clear from our analysis that a similar correlation exists for latent heat flux.

### *b. Diurnal cycle characteristics of precipitation features*

In this section, the diurnal cycle of MCS and sub-MCS precipitation features and their relation to environmental parameters are discussed. Figures 6 and 7 show selected MCS and sub-MCS precipitation feature attributes sampled by the ship radar in the EPIC and TEPPS regions. These metrics were chosen to represent fundamental horizontal and vertical characteristics of precipitation features in both regions.

#### 1) MCS FEATURES

As shown in Fig. 6, MCSs dominate the precipitation feature statistics in both the EPIC and TEPPS domains. The magnitude and amplitude variations of EPIC MCS rainfall characteristics are generally larger than in TEPPS MCSs across the diurnal cycle. This is consistent with the CAPE patterns shown in Fig. 5, indicating that the EPIC environment is more conducive to producing rainfall systems with more intense updrafts and enhanced mixed phase microphysical processes compared to TEPPS (CNR07). EPIC MCS features start increasing in midafternoon, reaching peak intensity in terms of rain rate and convective fraction (Figs. 6a,b) in the late night–early morning, in agreement with the overall CAPE pattern (Fig. 5). MCS maximum echo top height exhibits a broad maximum through the late

[2] The timing of the peak SST is sensitive to the time resolution used to represent the diurnal cycle. Tests with higher time resolution showed that the peak occurs between 1800 and 1900 LT.

[3] The role of nonconvective clouds in modulating SSTs during SMO periods cannot be ruled out. Examination of *RHB* features with no convective pixels (not shown) revealed a higher prevalence in the afternoon and evening hours over TEPPS compared to EPIC. Although these features have no discernable impact on rainfall statistics (see CNR07), they may play a role in modulating the amplitude of SSTs during light wind periods.

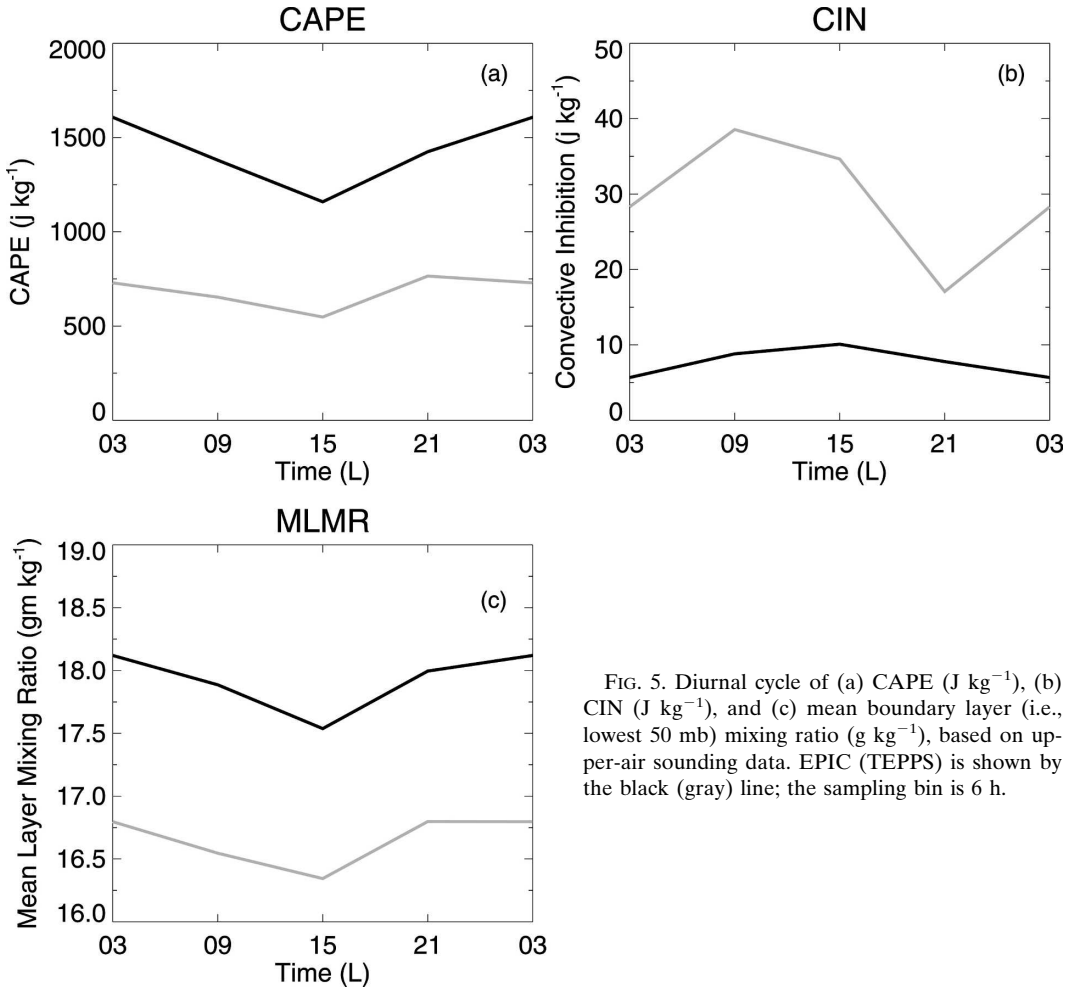


FIG. 5. Diurnal cycle of (a) CAPE (J $kg^{-1}$), (b) CIN (J $kg^{-1}$), and (c) mean boundary layer (i.e., lowest 50 mb) mixing ratio (g $kg^{-1}$), based on upper-air sounding data. EPIC (TEPPS) is shown by the black (gray) line; the sampling bin is 6 h.

night–early morning hours. Similar timing of peak rain rates and echo top heights were observed by rain gauges and cloud radar on board the *RHB* during EPIC (Raymond et al. 2004). EPIC MCS rain area and volume[4] (Figs. 6d,e) show broad maxima, extending from late night–early morning through the midmorning as these systems expand with and develop more stratiform echo (identified as a decrease in convective fraction; see Fig. 6b). This midmorning period also coincides with the maximum number of MCS occurrences (Fig. 6f).

These EPIC rainfall characteristics are in broad agreement with buoy observations reported for the east Pacific (Serra and McPhaden 2004) and with ship-based radar observations in the west Pacific during TOGA COARE (Sui et al. 1997; Short et al. 1997) and ground-based radar observations in the central Pacific during KWAJEX (Yuter et al. 2005). However, the peak amplitude of rain area in the west and central Pacific studies did not extend past sunrise, as is shown for EPIC. Sensitivity studies showed that even when the time bin used in this study was reduced to more closely match the west and central Pacific studies (1–2 h), the peak MCS rain area in the EPIC region extends past sunrise. Given that both the TOGA COARE and EPIC experiments were conducted over tropical oceans, which typically display late night–early morning maxima in rain rate (Yang and Smith 2006), the reason for the extension of the EPIC rainfall area and accumulation past sunrise requires explanation.

Insight into the latter rain area results may be obtained from previous satellite studies of rainfall in the global tropics. Specifically, investigations by Garreaud and Wallace (1997), Janowiak et al. (1994), Yang and Slingo (2001), Sorooshian et al. (2002), and Nesbitt and

[4] Following Mohr et al. (1999), Nesbitt and Zipser (2003), and CNR07, volumetric rainfall is defined as the integrated sum of rain rates for each precipitation feature per unit time.

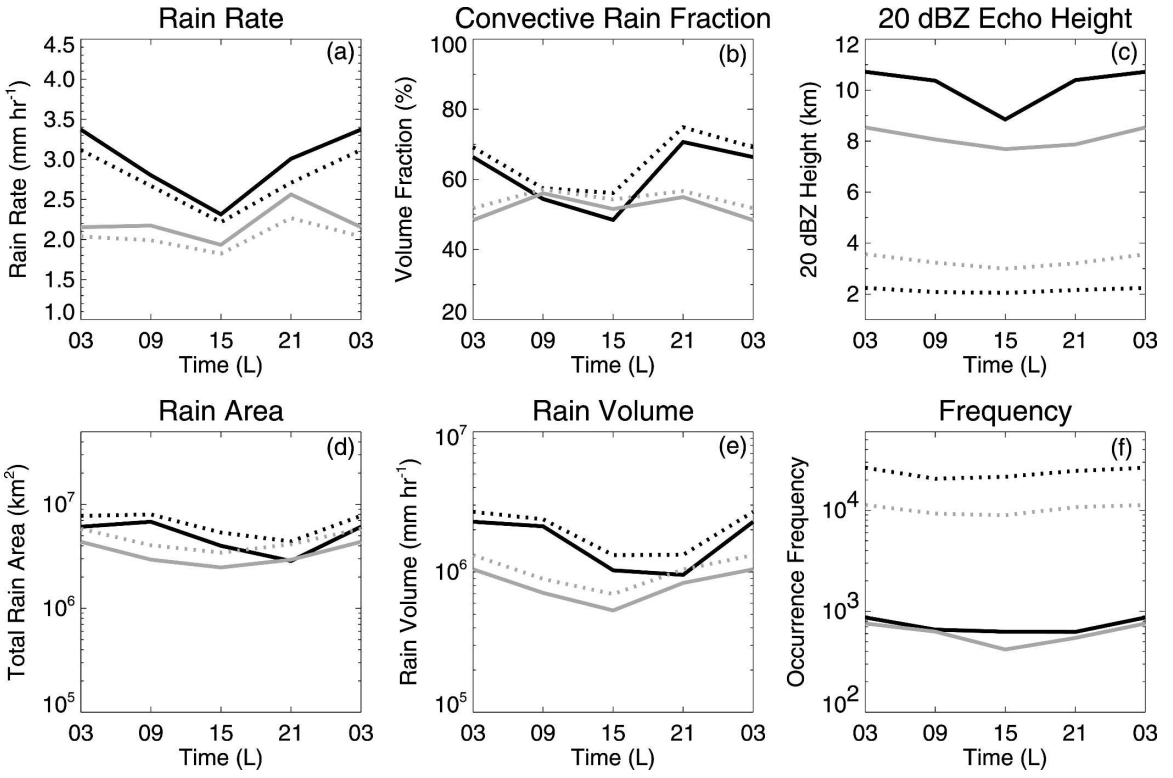


FIG. 6. Diurnal variability of all (sub-MCS and MCS combined) and MCS-only precipitation feature parameters observed from the *RHB* radar: (a) rain rate (mm $h^{-1}$), (b) convective fraction (%), (c) mean maximum 20-dBZ height (km), (d) rain area ($km^2$), (e) rain volume (mm $h^{-1}$), and (f) frequency of occurrence. Solid and dotted lines indicate MCS-only and all precipitation features, respectively. Black and gray lines indicate EPIC and TEPPS data, respectively.

Zipser (2003) have all shown a consistent pattern of maximum rainfall in the late afternoon–evening hours over the Central American landmass, transitioning to early morning over the adjacent east Pacific Ocean. This variation in the diurnal cycle of precipitation from land to ocean is shown in Fig. 1, based on a harmonic analysis of combined satellite microwave rain-rate estimates. The data in Fig. 1 indicate that convection tends to be present over the high terrain in Central America in the afternoon–evening and that signal in rainfall appears to propagate southwest, arriving within the EPIC domain between about 0600 and 1200 LT. Interestingly, the magnitude and spatial pattern of the diurnal harmonic analysis suggests that the EPIC region is situated in a transition region where the land-initiated signal begins to lose coherence over the open ocean. The propagation observed in Fig. 1 is consistent with a gravity wave propagation mechanism suggested by Yang and Slingo (2001). In this case, a phase speed of ~10 m $s^{-1}$ is implied based on analysis of Fig. 1. A gravity wave mechanism was also proposed by Mapes et al. (2003) to explain diurnal oscillations of convection between land and sea in the Panama Bight region of Central America, although the phase speed (~15 m $s^{-1}$) was larger than the propagation speed in our study. More detailed comparisons between diurnal cycle results for satellite and ship radar are presented below in section 3c.

On the scale of the *RHB* radar, there is no clear evidence of diurnal propagation across the EPIC domain (Fig. 8). This figure shows the spatial distribution of rain volume for MCS features.[5] The rainfall distribution in Fig. 8 shows that during the EPIC field program the eastern portion of the EPIC domain received more rain than the western portion across the diurnal cycle. Because of the relatively short time period of the experiment, however, it is likely that rainfall from individual precipitation features could swamp any climatological trend apparent from the southwesterly propagation of convection as seen by TRMM. Examination of OLR time–longitude plots (e.g., Petersen et al. 2003) reveal that the rainfall distribution sampled during

[5] Sub-MCSs did not show any discernable patterns in rain volume distribution across the EPIC domain.

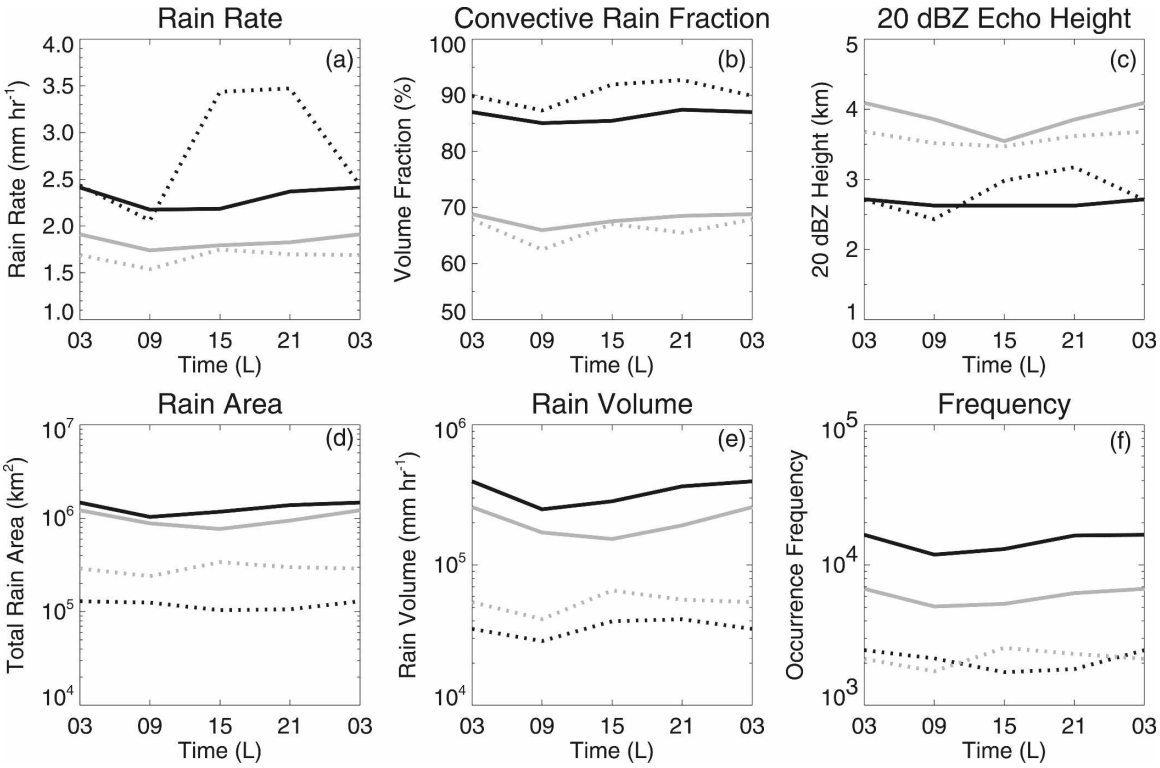


FIG. 7. Same as Fig. 6, but for subMCSs only. Solid (dashed) lines indicate all-data (SMO) periods.

EPIC was likely a consequence of the ship position relative to easterly wave passages during the field program.

As noted above, the Petersen et al. study has shown that convection observed during the EPIC campaign was significantly modulated by the passage of easterly waves. More recently, Pereira and Rutledge (2006) partitioned the EPIC radar data relative to easterly wave trough passages and found that during periods when the radar sampled rearward of the easterly wave trough axis (i.e., in the southerly regime), deep convective echo top heights and rain area and volume peaked near sunrise. In contrast, deep convective area and volume peaked earlier in the morning ahead of the easterly wave trough axis (i.e., in the northerly regime). As expected, the EPIC MCS diurnal patterns presented herein reflect a mix of regimes examined in Pereira and Rutledge (2006). For example, the broad maxima in echo top height and rain area presented in Fig. 6 reflect a combination of northerly and southerly regime signatures.

Similar to EPIC, TEPPS MCSs dominate the rainfall volume contribution across the diurnal cycle (Fig. 6). Moreover, MCS rainfall in both regions starts increasing during the midafternoon hours. However, TEPPS MCSs show less diurnal amplitude variability and generally achieve maxima in their feature-sampled characteristics earlier compared to EPIC. For example, TEPPS MCS rain rates peak in the evening, and rain area and rain volume maxima occur in the late night–early morning hours, one sampling bin (6 h) prior to EPIC. The shift to earlier times with respect to EPIC is consistent with the diurnal pattern of CAPE shown in Fig. 5. These results are in broad agreement with TRMM observations of MCSs across the tropical Pacific (Nesbitt and Zipser 2003). Unlike EPIC, the *RHB* data did not indicate that TEPPS MCSs produced a region of pronounced rainfall accumulation or a discernable migration pattern of rainfall across the domain (not shown).

### 2) SUB-MCS FEATURES

The diurnal cycle of sub-MCSs are shown in Fig. 7 for both the all-data and SMO periods. By definition, sub-MCSs are smaller than MCSs, ranging in size from individual cells to small groups of cells. As such, sub-MCSs would be expected to contain larger convective fractions, undergo less evolution in terms of size, rainfall volume, and maximum echo top heights, and have diurnal rainfall characteristics that are not necessarily in phase with MCSs. This is reflected in the Fig. 7 plots by the smaller amplitude of diurnal cycle characteristics

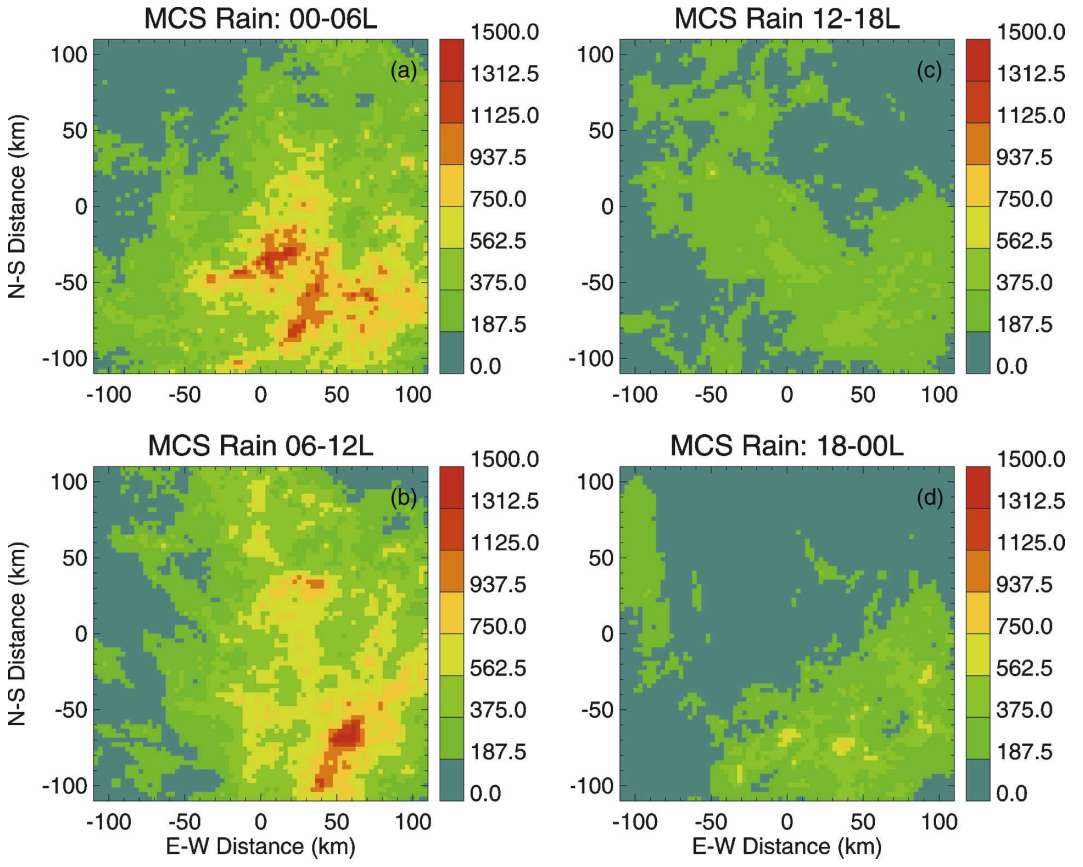


FIG. 8. Diurnal cycle of MCS rain volume distribution across the EPIC domain sampled by the *RHB* radar.

compared to MCSs. This change in diurnal amplitude and phase with precipitation area has also been observed in satellite IR data (Mapes and Houze 1993; Chen et al. 1996).

In EPIC, the sub-MCS features for the entire dataset start increasing in rain rate (Fig. 7a), convective fraction (Fig. 7b), size (Fig. 7d), accumulation Fig. 7e), and frequency (Fig. 7f) in midmorning, in phase with the solar insolation cycle. The maxima occur over a broad period extending from evening through the late night–early morning hours. Unlike the other parameters shown in Fig. 7, EPIC echo top heights show very little diurnal variability, at least when the all-data set is considered (Fig. 7c). This may result from the impact of dry layer intrusions during EPIC (Zuidema et al. 2006), which had a pronounced influence on the echo top characteristics of sub-MCSs (CNR07).

The main difference between sub-MCSs in the TEPPS and EPIC regions is that sub-MCS maximum echo top height and rain area and volume in TEPPS do not start increasing until midafternoon. Thus, although TEPPS sub-MCSs become more numerous throughout the day (as in EPIC), they do not grow much in size until the afternoon hours. The lack of growth until afternoon is coincident with the large CIN in the TEPPS region in the midmorning hours (Fig. 5b) and suggests that more thermal forcing is required for sub-MCSs to overcome the larger inhibition in the TEPPS region and grow upscale.

During SMO periods, the trend in sub-MCS features appears to be closely tied to the cycle of solar insolation. In EPIC, sub-MCS rain rates exhibit a pronounced peak in the midafternoon to evening, consistent with trends in SST and surface fluxes during SMO periods (Fig. 4). A similar pattern is observed in TEPPS sub-MCS rain rates, although the amplitude changes are smaller. This is not surprising, given the weaker SST and surface flux diurnal modulation during TEPPS SMO periods compared to EPIC. Both the EPIC and TEPPS results suggest that during relatively light wind conditions, sub-MCSs respond to surface heating in a similar way to land-based convection, although the magnitude is smaller because of the weaker forcing. Similar observations have been observed in the tropical west Pacific (Sui et al. 1997; Johnson et al. 2001; Chen et al. 1996). The main difference between the all-data

and SMO period sub-MCSs is that the peak of the former extends to the late night–early morning hours, closer to the peak of MCSs. This suggests that many of the sub-MCSs identified in this analysis are either precursors or remnants of MCSs. The simultaneous peak occurrence of both large and small cloud systems in the late night–early morning hours was also observed in the west Pacific during TOGA COARE (Chen and Houze 1997). As noted by Chen and Houze (1997), small cloud systems like sub-MCSs can be favored during periods of MCS activity because of the occurrence of convective outflows associated with the large systems.

### c. Comparison with satellite observations

In this section, we examine differences between multiyear satellite and the *RHB* field program estimates of precipitation over the EPIC and TEPPS domains. We start with the traditional proxy of IR brightness temperature. IR brightness temperature in satellite imagery is often used to estimate rainfall over a large range of time scales (Adler and Negri 1988; Janowiak and Arkin 1991). Here, we examine changes in the probability distributions of IR brightness temperature across the diurnal cycle. Histograms of IR brightness temperature at 6-h intervals, using combined data from July–September 2000–05 within a $5° \times 5°$ box surrounding each field campaign, are shown in Fig. 9. Although the IR fraction does not exactly correspond to any of the *RHB* observations shown in Figs. 5 and 6, it is expected that rain area and mean maximum echo top height would be the most comparable statistics. IR brightness temperatures below about 210 K have been shown by Mapes and Houze (1993) to correspond to areas of deep, organized convection (i.e., MCSs) and are hereafter referred to as deep clouds. IR brightness temperatures above this threshold represent successively higher-temperature clouds with lower echo tops.

In the EPIC region, deep clouds occur most often in the midmorning (Fig. 9a). Although the timing of these deep clouds is shifted several hours later compared to similar observations from the west Pacific (Chen et al. 1996; Hall and VonderHaar 1999), they are quite consistent with the EPIC MCS rain area and echo top height results shown in Fig. 6. As described in section 3b, the peak deep cloud in the EPIC region in midmorning may be related to land-based convection propagating into the domain and arriving near sunrise. In the TEPPS region, IR brightness temperatures below about 210 K occur less frequently than in EPIC and peak in the late night–early morning hours (Fig. 9b). Moreover, the difference in the relative frequency of TEPPS deep clouds across the diurnal cycle is smaller than in EPIC, in agreement with the relatively small amplitude changes in TEPPS MCS rain area and echo top heights shown in Fig. 6. We note that in both EPIC and TEPPS, the peak relative frequency of deep clouds occurs after the peak in CAPE (Fig. 5) and maximum rain rate (Fig. 6), similar to observations from the west Pacific (Petersen et al. 1996; Sui et al. 1997).

Figure 9 shows that the time of peak brightness temperature occurrence shifts to later in the day with increasing brightness temperature, indicating that higher-temperature clouds in the EPIC and TEPPS regions have a different diurnal pattern compared to deep, organized cloud systems (MCSs). Similar trends have been observed in the west Pacific (Mapes and Houze 1993). In both the EPIC and TEPPS regions, clouds with brightness temperatures 220–240 K occur most frequently in the midafternoon, and clouds with brightness temperatures in the 250–260-K range occur preferentially in the evening. Clouds with temperatures above about 260 K do not have a clear diurnal preference in either region.

Comparing the 220-K and higher-temperature trends with sub-MCS echo top heights and rain area shown in Fig. 7 is more complicated than with MCSs because of the small amplitude of the sub-MCS diurnal patterns and the fact that these higher IR temperature thresholds likely represent a mixture of cloud populations. We compare the all-data sub-MCSs rather than the sub-MCSs in SMO periods because only the former are likely to be captured in the multiyear satellite composite. As expected, comparisons of Figs. 7 and 9 show that there is not a clear correspondence between the sub-MCS diurnal precipitation patterns and the IR histograms in either region.

Because the TRMM PR carries a precipitation radar (Kummerow et al. 1998), a more direct comparison can be made with the *RHB* results described in section 3b. Comparisons between the ship radar and TRMM PR rainfall statistics are presented in Fig. 10 for MCSs and in Fig. 11 for sub-MCSs. As shown in these figures, there are many more *RHB* samples compared to the PR. This is especially true for MCSs, where the PR sample consists of $<200$ samples in each time bin (Fig. 10). Although sensitivity tests with temporal and spatial averaging did not reveal significant changes in the PR MCS diurnal characteristics, we nevertheless place less confidence in these results than in the sub-MCSs results, which have several thousand samples in each time bin (Fig. 11).

We note that the TRMM PR feature identification threshold was 20 dB$Z$ compared to 10 dB$Z$ for the *RHB* (see section 2 for a discussion on how precipitation features are identified). The higher threshold for the PR results from the lower sensitivity of the satellite

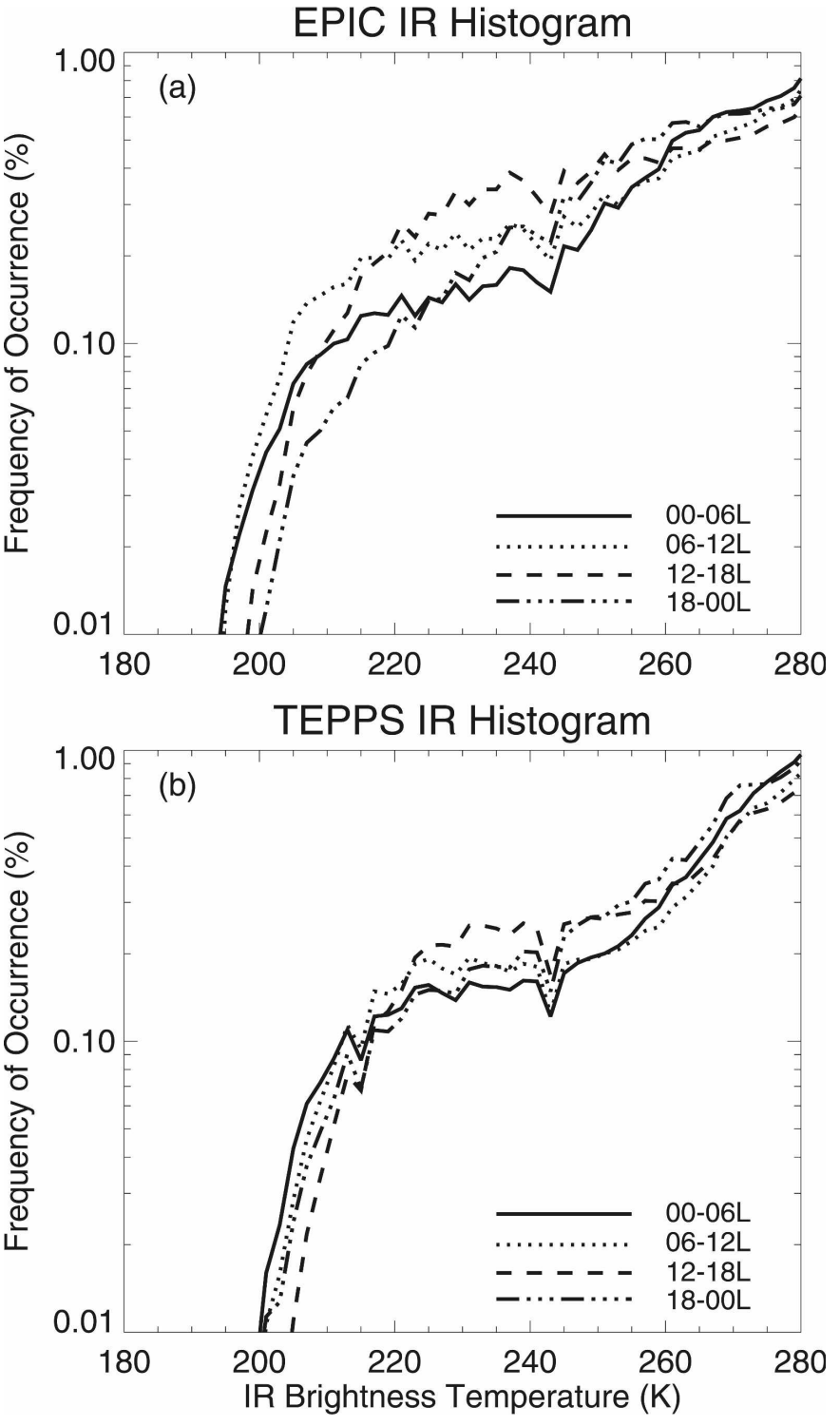


FIG. 9. IR brightness temperature histograms for the (a) EPIC and (b) TEPPS regions. Brightness temperatures are calculated within 5° × 5° boxes centered on the EPIC and TEPPS nominal field experiment locations, based on 2000–05 July–September data. Line types indicate IR brightness temperature histograms for different diurnal time periods as indicated in each plot. The resolution of the histograms is 2 K.

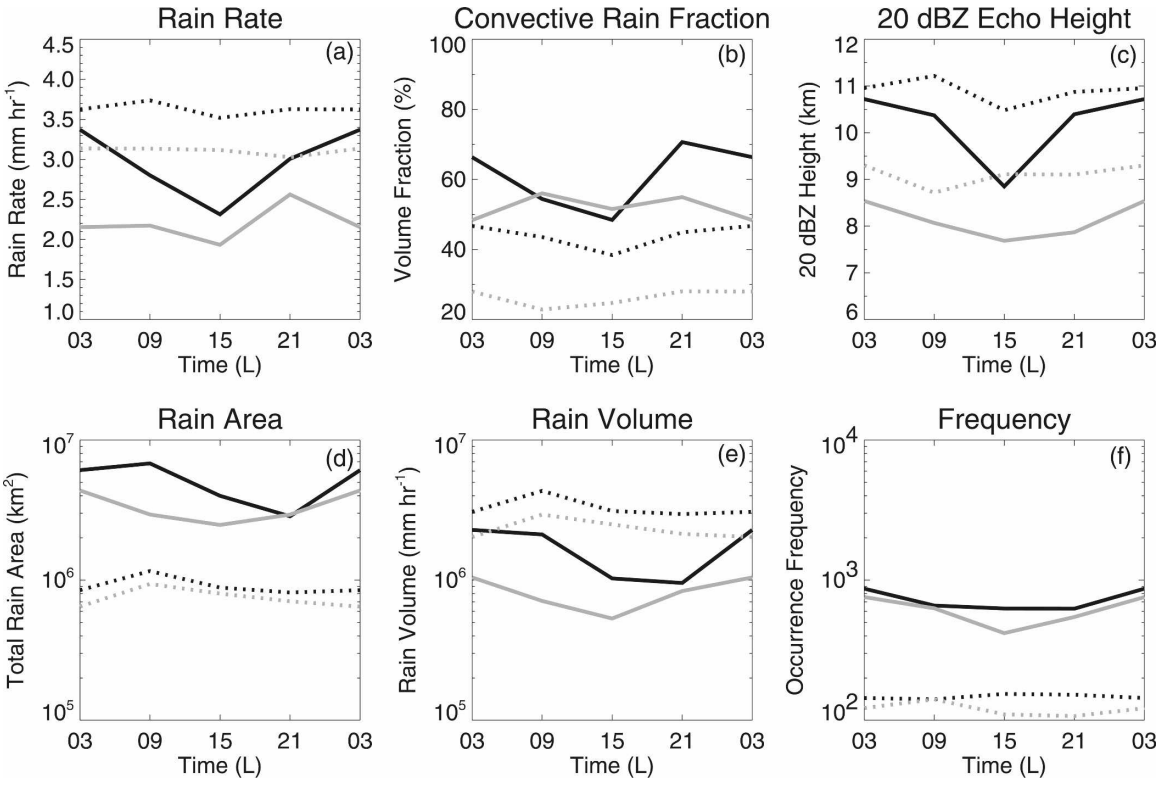


FIG. 10. Comparison of TRMM-PR and *RHB* rainfall parameters over the EPIC (black) and TEPPS (gray) domain for MCS features. TRMM-PR curves (dotted lines) represent 5° × 5° composite centered on the nominal location of the field campaigns. *RHB* data are indicated by the solid lines. (a)–(f) As in Fig. 6.

radar relative to the *RHB*. As in CNR07, sensitivity studies were performed, comparing the *RHB* features identified with a 10- or 20-dB*Z* threshold to the PR results. Although the magnitude of the parameters changes, the overall patterns remain the same, indicating that the results shown in Figs. 10 and 11 are robust. In general, changing the *RHB* threshold from 10 to 20 dB*Z* increases the magnitude of *RHB* rain rate and convective fraction and decreases echo top heights. However, the change has a negligible effect on rain area and volume. Here, we adopt the 10-dB*Z* threshold for the *RHB* data to be consistent with CNR07.

In terms of MCSs, Fig. 10 shows that the amplitude of diurnal variability is smaller for the satellite compared to the *RHB* observations in both regions for all of the parameters shown. The reason for the dampening of the PR diurnal amplitudes relative to the *RHB* values reflects the larger satellite sampling area and resulting variance across the region, the variability in rain statistics during the time period in which TRMM data was composited, and the relatively low temporal resolution of TRMM, as well as sampling error from TRMM's orbit (Bowman et al. 2005). CNR07 also noted that the TRMM data exhibited significant interannual and interseasonal variability over the 7 yr used in the satellite composite. Despite the variability in the satellite climatology, the TRMM PR and *RHB* MCS patterns in the EPIC region are in reasonable agreement for most parameters shown in Fig. 10. Both the ship and satellite radars show an increase in MCS activity through the midafternoon and evening hours, with maximum echo top heights, rain area, and volume in the morning hours (Figs. 10c–e). In terms of rain rate (Fig. 10a), both the *RHB* and PR indicate an increase starting in the midafternoon; however, the satellite data show a broader maxima, peaking later in the morning compared to the *RHB* late night–early morning peak.

Similar to EPIC, the diurnal cycle of PR-observed MCS rainfall characteristics has smaller amplitude compared to the *RHB* data in the TEPPS region. As shown in Fig. 10 and discussed previously in section 3b, TEPPS MCSs observed by the *RHB* increase in the midafternoon, reaching maximum intensity in terms of rain rate in the evening (Fig. 10a) and maximum echo top height and rain area and volume in the late night–early morning (Figs. 10c–e). However, the TRMM PR data suggests a later peak (midmorning) in MCS maximum echo top height and rain area and volume, together

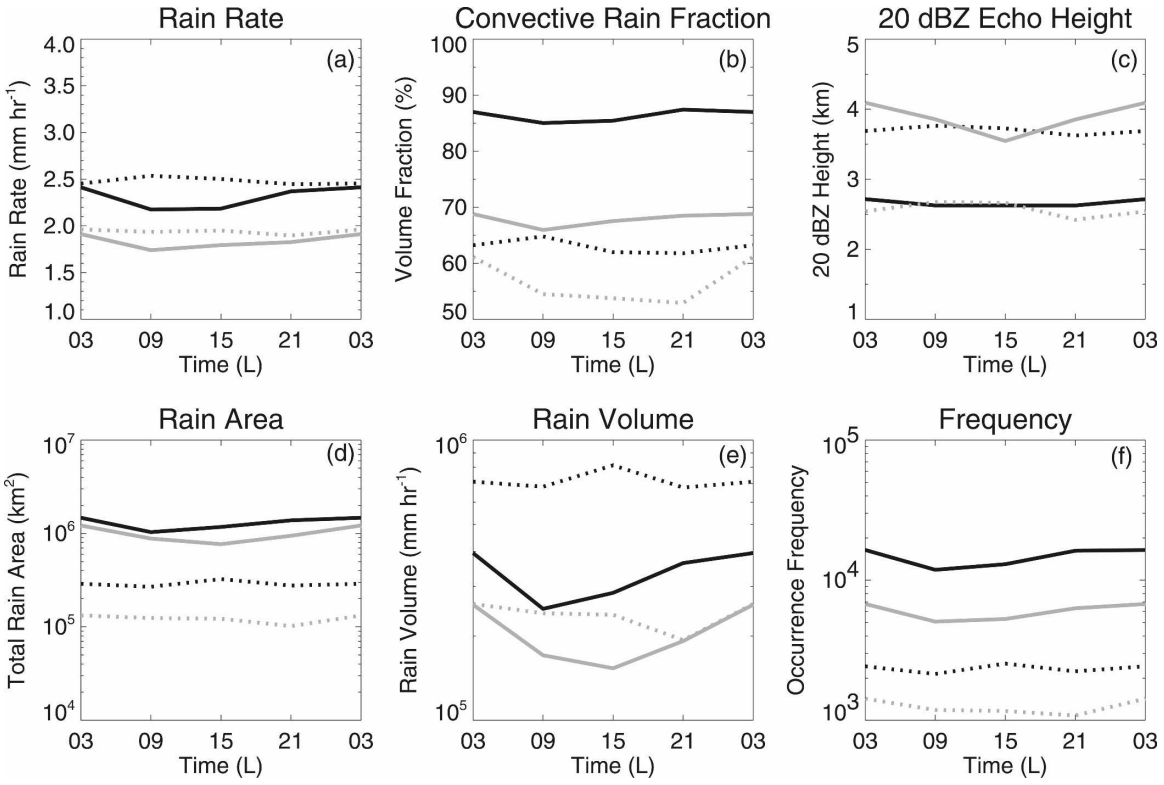


FIG. 11. Same as Fig. 10, but for sub-MCS features.

with a negligible change in rain rate across the diurnal cycle. The reason for the offset is not clear but may be a consequence of the fact that the diurnal amplitude in the TEPPS region is weak (as indicated by harmonic analysis in Fig. 1) and contains a limited number of PR samples (Fig. 10). An additional contribution to the *RHB* and PR differences in the TEPPS region may be due to the fact that the TEPPS campaign was conducted during an El Niño event (Yuter and Houze 2000), when it would be expected that the east Pacific ITCZ would shift position and become more active compared to non–El Niño years (CNR07). CNR07 found that MCSs sampled by the *RHB* and TRMM in the TEPPS region were in good agreement in terms of overall rainfall statistics; however, that study did not examine the diurnal cycle of rainfall characteristics.

To assess whether El Niño may have affected the diurnal cycle patterns, different satellite analysis boxes were constructed, spanning regions farther north of the TEPPS experiment and more central to the ITCZ in non–El Niño years. Although the magnitude of the parameters changes slightly, shifting the analysis box farther north or increasing the size had very little effect on the diurnal patterns shown in Fig. 10. All of the test boxes examined indicate a late evening–early morning maximum in rain rate, and echo tops and rain area peak after sunrise, similar to the patterns shown in Fig. 10. The amplitudes are weak in all cases.

As noted previously, the diurnal amplitude of sub-MCS features is small compared to MCSs; this is also observed in the TRMM PR data (Fig. 11). In the EPIC region, there are similar trends in terms of an increase in size, volume, and occurrence in the midmorning to midafternoon hours, but there are differences in the patterns in the evening to the late night–early morning period (Figs. 11d–f). Similar discrepancies occur in the TEPPS region. Apparently, the temporal and spatial variability of these features within the compositing region used in this study is sufficient to essentially wash out discernable patterns.

## 4. Summary

Using a combination of buoy, ship radar, sounding, and satellite data, this study has identified diurnal patterns of precipitation characteristics over two regions of the east Pacific where recent field programs were conducted (EPIC and TEPPS). Precipitation features were identified in radar data using an objective algorithm and separated into two classes: MCS and sub-MCS. The diurnal patterns of salient MCS and sub-MCS characteristics are illustrated in Fig. 12.

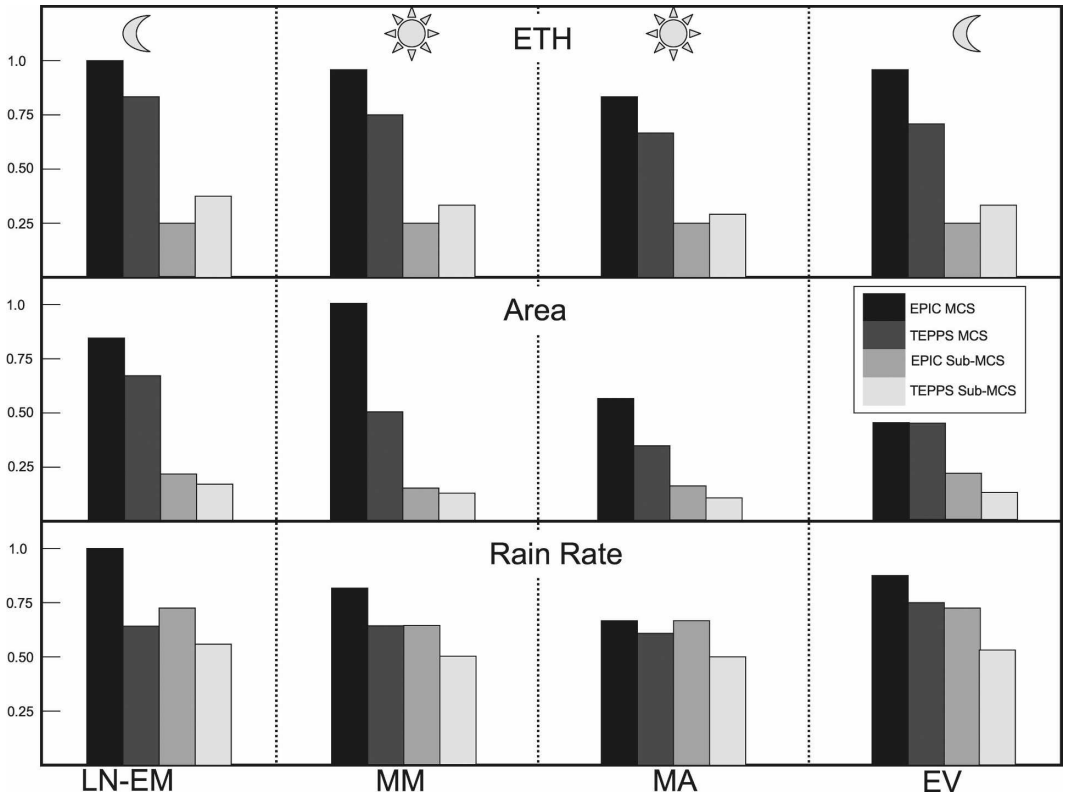


FIG. 12. Schematic showing diurnal evolution of selected feature characteristics: (top) mean maximum echo top height, (middle) area, and (bottom) rain rate. In each row, the bars are scaled relative to the maximum value over the diurnal cycle. LN–EM, MM, MA, and EV refer to late night–early morning, midmorning, midafternoon, and evening, respectively. In each panel, bars represent (from left to right) EPIC MCS, TEPPS MCS, EPIC sub-MCS, and TEPPS sub-MCS, as indicated by the legend in the far right panel of the middle row. Note that the sub-MCS bars refer to all-data periods.

In terms of MCS precipitation features, the EPIC region displayed a pronounced diurnal cycle of rain rate, convective fraction, rain area, and mean maximum echo top heights. These EPIC systems were shown to build through the afternoon hours, reaching maximum intensity in terms of rain rate in the late night–early morning. This pattern is consistent with the cycle of CAPE discerned in upper-air sounding data. Maxima in EPIC MCS rain area and accumulation were achieved in the midmorning after sunrise as organized systems spread out and developed stratiform components. The *RHB* radar data also indicated that the eastern portion of the EPIC region received appreciably more rainfall than the western portion over the course of the field program. At larger spatial scales, satellite datasets identified a precipitation signal originating in the afternoon–evening over high terrain in Central America, which appeared to propagate into the EPIC region during the morning hours. Thus, the phase of the diurnal signal in EPIC is modulated by land-based convection. A harmonic analysis of TRMM data showed that the EPIC domain occurs in the transition region where the land-generated signal becomes lost over the open ocean.

In contrast to EPIC, TEPPS was conducted in an open-ocean location far removed from land. TEPPS MCSs had a weaker diurnal signal, with maxima for precipitation characteristics occurring earlier with respect to EPIC. TEPPS MCSs achieved maximum rain rate in the evening and maximum rain area in the late night–early morning hours, similar to previous ship radar observations of oceanic convection in the tropical west Pacific. Both the EPIC and TEPPS *RHB*-observed patterns of MCS rain area and maximum echo top height are in good agreement with a 6-yr July–September climatology of IR deep cloud fraction in the regions. The EPIC *RHB* MCS results are also similar to a 7-yr climatology of TRMM-PR MCS precipitation features identified over the same 3-month period. However, the TEPPS region comparison of TRMM and *RHB* radar statistics showed more discrepancies, perhaps due to the fact that the TEPPS diurnal signal is

weak compared to EPIC. The fact that TEPPS was conducted in an El Niño year may have further complicated the comparison but appears to have only had a minor effect on the results. The relatively weak amplitude in the TEPPS observations suggests that model validation of the diurnal cycle in the TEPPS region would be more difficult than in EPIC because of the smaller amplitude of the diurnal signal in the precipitation characteristics.

Sub-MCS features were also examined, and their diurnal pattern was found to be more in phase with the cycle of solar insolation. This is especially true in the EPIC region during SMO periods when surface fluxes increased markedly in the afternoon hours, similar to observations from the tropical west Pacific. During these light wind periods, sub-MCSs increased starting in the midmorning and peaking in the evening, similar to convection over land. The TEPPS region also showed an afternoon increase in sub-MCS precipitation during SMO periods, albeit weaker than EPIC and consistent with less surface flux forcing during SMO conditions in TEPPS. When the all-data case was considered, sub-MCSs in both regions were found to reach maximum rainfall characteristics over a broad period extending from evening through late night–early morning, closer to the phase of MCSs. This suggests that sub-MCSs sampled outside SMO periods were enhanced through MCS processes such as outflow boundaries, similar to observations from the tropical west Pacific. Comparisons of sub-MCS rainfall metrics observed by satellite and ship radar were complicated by the small amplitudes of these features and were generally not as favorable as the MCS ones.

*Acknowledgments.* Dave Wolff at the NASA TRMM Office provided the QC algorithm for the EPIC and TEPPS ship radar data. Meghan Cronin and Chris Fairall provided the buoy data. Three anonymous reviewers provided helpful comments that improved the manuscript. The authors extend their appreciation to all of the people who helped collect data during the EPIC and TEPPS field campaigns. This work was supported by NSF Grants ATM-0002256 and ATM-0340544 and NASA Grants NAG5-13623, NAG5-9716, and NNG04GJ15G under Ramesh Kakar.

## REFERENCES

Adler, R. F., and A. J. Negri, 1988: A satellite infrared technique to estimate tropical convective and stratiform rainfall. *J. Appl. Meteor.,* **27,** 30–51.

Arakawa, A., 2004: The cumulus parameterization problem: Past, present, and future. *J. Climate,* **17,** 2493–2525.

Arkin, P. A., and B. N. Meisner, 1987: The relationship between large-scale convective rainfall and cold cloud over the Western Hemisphere during 1982–84. *Mon. Wea. Rev.,* **115,** 51–74.

Bowman, K. P., J. C. Collier, G. R. North, Q. Wu, E. Ha, and J. Hardin, 2005: Diurnal cycle of tropical precipitation in Tropical Rainfall Measuring Mission (TRMM) satellite and ocean buoy rain gauge data. *J. Geophys. Res.,* **110,** D21104, doi:10.1029/2005JD005763.

Chen, S. S., and R. A. Houze Jr., 1997: Diurnal variation and life cycle of deep convective systems over the tropical Pacific warm pool. *Quart. J. Roy. Meteor. Soc.,* **123,** 357–388.

——, ——, and B. E. Mapes, 1996: Multiscale variability of deep convection in relation to large-scale circulation in TOGA COARE. *J. Atmos. Sci.,* **53,** 1380–1409.

Cifelli, R., S. W. Nesbitt, S. A. Rutledge, W. A. Petersen, and S. Yuter, 2007: Radar characteristics of precipitation features in the EPIC and TEPPS regions of the east Pacific. *Mon. Wea. Rev.,* **135,** 1576–1595.

Cronin, M. F., and W. S. Kessler, 2002: Seasonal and interannual modulation of mixed layer variability at 0°, 110°W. *Deep-Sea Res.,* **49,** 1–17.

——, C. W. Fairall, and M. J. McPhaden, 2006: An assessment of buoy-derived and numerical weather prediction surface heat fluxes in the tropical Pacific. *J. Geophys. Res.,* **111,** C06038, doi:10.1029/2005JC003324.

Dai, A., 2001: Global precipitation and thunderstorm frequencies. Part II: Diurnal variations. *J. Climate,* **14,** 1112–1128.

——, and K. E. Trenberth, 2004: The diurnal cycle and its depiction in the Community Climate System Model. *J. Climate,* **17,** 930–951.

DeMaria, M., 1985: Linear response of a stratified tropical atmosphere to convective forcing. *J. Atmos. Sci.,* **42,** 1944–1959.

Garreaud, R., and J. M. Wallace, 1997: The diurnal march of convective cloudiness over the Americas. *Mon. Wea. Rev.,* **125,** 3157–3171.

Gray, W., and R. W. Jacobson, 1977: Diurnal variation of deep cumulus convection. *Mon. Wea. Rev.,* **105,** 1171–1188.

Hall, T. J., and T. H. Vonder Haar, 1999: The diurnal cycle of west Pacific deep convection and its relation to the spatial and temporal variation of tropical MCSs. *J. Atmos. Sci.,* **56,** 3401–3415.

Hartmann, D. L., H. H. Hendon, and R. A. Houze Jr., 1984: Some implications of the mesoscale circulations in tropical cloud clusters for large-scale dynamics and climate. *J. Atmos. Sci.,* **41,** 113–121.

Hendon, H. H., and K. Woodberry, 1993: The diurnal cycle of tropical convection. *J. Geophys. Res.,* **98,** 16 623–16 637.

Houze, R. A., Jr., S. G. Geotis, F. D. Marks Jr., and A. K. West, 1981: Winter monsoon convection in the vicinity of north Borneo. Part I: Structure and time variation of the clouds and precipitation. *Mon. Wea. Rev.,* **109,** 1595–1614.

Janowiak, J. E., and P. A. Arkin, 1991: Rainfall variations in the tropics during 1986-1989, as estimated from observations of cloud-top temperature. *J. Geophys. Res.,* **96,** 3359–3373.

——, ——, and M. L. Morrissey, 1994: An examination of the diurnal cycle in oceanic tropical rainfall using satellite and in situ data. *Mon. Wea. Rev.,* **122,** 2296–2311.

——, ——, P. Xie, M. L. Morrissey, and D. R. Legates, 1995: An examination of the east Pacific ITCZ rainfall distribution. *J. Climate,* **8,** 2810–2823.

——, R. J. Joyce, and Y. Yarosh, 2001: A real-time global half-hourly pixel-resolution infrared dataset and its applications. *Bull. Amer. Meteor. Soc.,* **82,** 205–217.

Johnson, R. H., P. E. Ciesielski, and J. A. Cotturone, 2001: Mul-

tiscale variability of the atmospheric mixed layer over the western Pacific warm pool. *J. Atmos. Sci.,* **58,** 2729–2750.

——, S. L. Aves, S. L. Nesbitt, and P. E. Ciesielski, 2004: The diurnal cycle of precipitation over the northern South China Sea. *Proc. 2nd TRMM Int. Science Conf.,* Nara, Japan, Japan Aerospace Exploration Agency, 4.3.

Kiladis, G. N., and M. Wheeler, 1995: Horizontal and vertical structure of observed tropospheric equatorial Rossby waves. *J. Geophys. Res.,* **100,** 22 981–22 997.

Kummerow, C., W. Barnes, T. Kozu, J. Shiue, and J. Simpson, 1998: The Tropical Rainfall Measuring Mission (TRMM) sensor package. *J. Atmos. Oceanic Technol.,* **15,** 809–817.

Lin, X., D. A. Randall, and L. D. Fowler, 2000: Diurnal variability of the hydrologic cycle and radiative fluxes: Comparisons between observations and a GCM. *J. Climate,* **13,** 4159–4179.

Loehrer, S. M., T. A. Edmands, and J. A. Moore, 1996: TOGA COARE upper-air sounding data archive: Development and quality control procedures. *Bull. Amer. Meteor. Soc.,* **77,** 2651–2671.

Mapes, B. E., and R. A. Houze Jr., 1993: Cloud clusters and superclusters over the oceanic warm pool. *Mon. Wea. Rev.,* **121,** 1398–1416.

——, T. T. Warner, and M. Xu, 2003: Diurnal patterns of rainfall in northwestern South America. Part III: Diurnal gravity waves and nocturnal convection offshore. *Mon. Wea. Rev.,* **131,** 830–844.

McPhaden, M. J., and Coauthors, 1998: The tropical ocean–global atmosphere (TOGA) observing system: A decade of progress. *J. Geophys. Res.,* **103,** 14 169–14 240.

Mechoso, C. R., and Coauthors, 1995: The seasonal cycle over the tropical Pacific in coupled ocean–atmosphere general circulation models. *Mon. Wea. Rev.,* **123,** 2825–2838.

Mohr, K. I., J. S. Famiglietti, and E. J. Zipser, 1999: The contribution to tropical rainfall with respect to convective system type, size, and intensity estimated from the 85-GHz ice-scattering signature. *J. Appl. Meteor.,* **38,** 596–606.

Nesbitt, S. W., and E. J. Zipser, 2003: The diurnal cycle of rainfall and convective intensity according to three years of TRMM measurements. *J. Climate,* **16,** 1456–1475.

Pereira, L. G., and S. A. Rutledge, 2006: Diurnal cycle of shallow and deep convection for a tropical land and an ocean environment and its relationship to synoptic wind regimes. *Mon. Wea. Rev.,* **134,** 2688–2701.

Petersen, W. A., S. A. Rutledge, and R. E. Orville, 1996: Cloud-to-ground lightning observations from TOGA COARE: Selected results and lightning location algorithms. *Mon. Wea. Rev.,* **124,** 602–620.

——, R. Cifelli, D. J. Boccippio, S. A. Rutledge, and C. Fairall, 2003: Convection and easterly wave structures in the eastern Pacific warm pool during EPIC-2001. *J. Atmos. Sci.,* **60,** 1754–1773.

Raymond, D. J., G. B. Raga, C. S. Bretherton, J. Molinari, C. López-Carrillo, and Z. Fuchs, 2003: Convective forcing in the intertropical convergence zone of the eastern Pacific. *J. Atmos. Sci.,* **60,** 2064–2082.

——, and Coauthors, 2004: EPIC2001 and the coupled ocean–atmosphere system of the tropical east Pacific. *Bull. Amer. Meteor. Soc.,* **85,** 1341–1354.

Riehl, H., and J. S. Malkus, 1958: On the heat balance of the equatorial trough zone. *Geophysica,* **6,** 503–538.

Serra, Y. L., and R. A. Houze Jr., 2002: Observations of variability on synoptic timescales in the east Pacific ITCZ. *J. Atmos. Sci.,* **59,** 1723–1743.

——, and M. J. McPhaden, 2004: In situ observations of diurnal variability in rainfall over the tropical Pacific and Atlantic oceans. *J. Climate,* **17,** 3496–3509.

Short, D. A., P. A. Kucera, B. S. Ferrier, J. C. Gerlach, S. A. Rutledge, and O. W. Thiele, 1997: Shipboard radar rainfall patterns within the TOGA COARE IFA. *Bull. Amer. Meteor. Soc.,* **78,** 2817–2836.

Sorooshian, S., X. Gao, K. Hsu, R. A. Maddox, Y. Hong, H. V. Gupta, and B. Imam, 2002: Diurnal variability of tropical rainfall retrieved from combined GOES and TRMM satellite information. *J. Climate,* **15,** 983–1001.

Straub, K. H., and G. N. Kiladis, 2002: Observations of a convectively coupled Kelvin wave in the eastern Pacific ITCZ. *J. Atmos. Sci.,* **59,** 30–53.

Su, H., and J. D. Neelin, 2003: The scatter in tropical average precipitation anomalies. *J. Climate,* **16,** 3966–3977.

——, ——, and C. Chou, 2001: Tropical teleconnection and local response to SST anomalies during the 1997–1998 El Niño. *J. Geophys. Res.,* **106,** 20 025–20 043.

Sui, C.-H., K.-M. Lau, Y. M. Takayabu, and D. A. Short, 1997: Diurnal variations in tropical oceanic cumulus convection during TOGA COARE. *J. Atmos. Sci.,* **54,** 639–655.

Yang, G.-Y., and J. Slingo, 2001: The diurnal cycle in the tropics. *Mon. Wea. Rev.,* **129,** 784–801.

Yang, S., and E. A. Smith, 2006: Mechanisms for diurnal variability of global tropical rainfall observed from TRMM. *J. Climate,* **19,** 5190–5226.

Yuter, S. E., and R. A. Houze Jr., 1998: The natural variability of precipitating clouds over the western Pacific warm pool. *Quart. J. Roy. Meteor. Soc.,* **124,** 53–99.

——, and ——, 2000: The 1997 Pan American Climate Studies Tropical Eastern Pacific Process Study. Part I: ITCZ region. *Bull. Amer. Meteor. Soc.,* **81,** 451–481.

——, ——, E. A. Smith, T. T. Wilheit, and E. Zipser, 2005: Physical characterization of tropical oceanic convection observed in KWAJEX. *J. Appl. Meteor.,* **44,** 385–415.

Zuidema, P., B. Mapes, J. Lin, C. Fairall, and G. Wick, 2006: The interaction of clouds and dry air in the eastern tropical Pacific. *J. Climate,* **19,** 4531–4544.